communications physics

ARTICLE

https://doi.org/10.1038/s42005-022-00989-x OPEN

Gain-controlled broadband tuneability in self-mode-locked Thulium-doped fibre laser

Dennis C. Kirsch[1✉], Anastasia Bednyakova[2], Petr Varak[3], Pavel Honzatko[3], Benoit Cadier[4], Thierry Robin[4], Andrei Fotiadi[5,6], Pavel Peterka[3] & Maria Chernysheva[1]

Ensuring self-driven mode-locking and broadband wavelength tuneability in all-fibre-integrated femtosecond laser sources enables a new level of their versatility and extends areas of their applications. Principle limitations for this are traditionally available ultrafast modulators and tuneability techniques. Here, we exploit Thulium-doped fibre to perform three roles in the cavity: laser gain, saturable absorber, and tuneability element via controlling its excitation level. We confirmed that Tm-doped fibre saturable absorption is defined by a reinforced quenching of Tm^{3+} pairs. As a result, we present both numerically and experimentally a highly stable sub-picosecond pulse generation with a ~90 nm tuneability range spanning from 1873 to 1962 nm via adjusting the cavity feedback. The maximum laser efficiency corresponds to 25% cavity feedback, enabling the highest output energy of 1 nJ in 600-fs solitons at 1877 nm. Overall, the presented laser system establishes a compact and straightforward approach for ultrafast generation, which can be translated to other fibre laser operation wavelengths.

[1] Ultrafast Fibre Laser, Leibniz Institute of Photonic Technology, Albert-Einstein-Str. 9, 07745 Jena, Germany. [2] Novosibirsk State University, 1 Pirogova str., Novosibirsk 630090, Russia. [3] Institute of Photonics and Electronics, The Czech Academy of Sciences, Chaberska 57, 18251 Prague, Czechia. [4] iXblue Photonics, Rue Paul Sabatier, 22300 Lannion, France. [5] Ulyanovsk State University, 42, Leo Tolstoy Street, Ulyanovsk 432017, Russia. [6] Electromagnetism and Telecommunication Department, University of Mons, B-7000 Mons, Belgium. ✉email: dennis.kirsch@leibniz-ipht.de

Strengthening of laser technology's position in scientific, industrial and daily life applications relies on the system performance, specifically on how flexible it can adapt to the broad range of requirements. In this perspective, Thulium-doped fibres enable the exploration of a highly desirable broad wavelength range, spanning over ~350 nm around 2 μm. Such unique operation bandwidth has placed these fibre laser systems at the forefront of diverse applications. Environmental monitoring of greenhouse gases[1], polymer or semiconductor machining[2], optical coherence tomography[3], nonlinear microscopy[4], and optical communication[5]—these are just a handful of the ultrafast laser tasks which have been enabled by or enhanced with the Tm-doped fibre systems development. Versatile, tuneable, and highly integrated turnkey ultrafast fibre laser solutions are of high demand to empower emerging technological platforms and reinforce their rapid progress towards hand-held instruments. Yet, the development of such instruments is mainly obstructed by the imperfections and limitations of specific essential components that exhibit saturable absorption and wavelength tuneability behaviour.

The most notable saturable absorbers, which ensure phase-locking of longitudinal cavity modes, are SESAMs (e.g. GaSb)[6], carbon nanomaterials[7], transition metal dichalcogenides[8], or MXene[9]. However, besides poor long-term reliability and power-handling, their performance in the short-wave infra-red (SWIR) wavelength range lags behind their operation at Near-IR. At the same time, widely used all-fibre artificial modulators based on the optical Kerr effect, such as nonlinear polarisation evolution (NPE), nonlinear loop mirrors or nonlinear multimode interference, suffer from the diminished nonlinearity of optical fibres at the SWIR. This limitation leads to a high self-starting threshold and the necessity to design complex cavity configurations[10].

In such context, the visionary idea of mode-locked fibre lasers involving no apparent saturable absorber in the cavity has been validated through nonlinear coupling between cores in multi-core fibres[11], inter-mode beating[12], or self-absorption in a gain fibre. Conventionally, the latter has been considered undesirable instability in continuous-wave fibre lasers[13] and was only later studied as an ultrashort pulse formation mechanism. The saturable absorption behaviour of unexcited rare-earth-doped fibres has been mainly exploited at bandwidths where their absorption cross-section covers the emission cross-section of separate gain fibre[14,15]. Due to the slow recovery time of such a saturable absorption mechanism, the reciprocity of self-phase modulation (SPM) and anomalous group-delay dispersion became imperative for soliton shaping[16]. So far, only a few works have reported the gain fibre saturable absorption dynamics to enable the formation of few-picosecond mode-locked pulses as long as was assisted by SPM accumulated over tens of metres long laser cavities[17–19].

At the same time, a broad range of laser generation wavelength tuneability up to 300 nm (1733–2033 nm), demonstrated in Tm-doped fibre lasers[20], is generally implemented using bulk acousto-optic tunable filters[21], diffraction gratings[22], volume Bragg gratings[23], or planar semiconductor chips[24]. For this reason, the benefits of laser operation tuneability come at the cost of generation stability and substantial insertion losses. Thus, the possibilities of shaping and manipulating the laser generation through the interplay of intrinsic intracavity phenomena have recently become a topic of intensive experimental and theoretical investigation[25–27]. It is worth mentioning that bending of active fibre presents another technique for the operation wavelength variation, demonstrating 152 nm wavelength tuneability from 1740 to 1892 nm[28]. However, the fundamental principle of such tuneability relies on wavelength-selective losses, suppressing spontaneous emission at the longer edge of the gain spectrum. Such tuneability mechanism has been ensured by the proper design of a bend-sensitive W-type active fibre, in which cladding comprises a depressed ring with a lower refractive index. Importantly, like any other technique relying on loss introduction, these results came at the price of reduced laser efficiency. With up to 1.3 W pump power, the maximum average output power reached only 4.5 mW. Additionally, the realisation of continuous sweeping of the central laser wavelength by changing the fibre coiling radius introduces another level of complexity to the system.

Specifically, in Tm-doped fibre as quasi-three-level systems, the equilibrium between emission and absorption and, thus, the profile of the gain spectrum $g(\lambda)$ is governed by the lower N_1 and excited laser level N_2 population fractions (Supplementary Note 1). Supplementary Fig. S1b predicts spectral gain profiles of Tm-doped fibre (used in further investigations) to red-shift at higher excitation level[29,30]. The control of the laser cavity Q-factor allows efficient governing of an excitation level of the gain, leveraging output power and laser generation wavelength. The control of the Q-factor can be implemented, for example, by changing the active fibre length or its doping concentration[31], or by altering cavity loss through implemented attenuation[32,33] or controlling laser feedback[34]. The cavity feedback control has been investigated mainly for the relatively narrow band of the Erbium gain[34–36]. Active fibres with broader gain spectra hold the true potential since the actual tuning range is built by the shape and overlap of the emission and absorption cross-sections. Nevertheless, the presented attempts to control wavelength-independent losses have not demonstrated remarkable tuneability ranges in Tm-doped fibre lasers. While theoretical work predicted the possibility of achieving a 105 nm tuneability in a continuous-wave generation, only 36[32] and 48 nm[33] tuneability has been achieved in the experiment. Still, continuous wavelength tuneability in ultrafast Tm-doped fibre lasers remains largely unexplored.

In this work, we explore the phenomenon of self-mode-locking and enable tuneable ultrashort pulse generation by manipulating the gain excitation level, omitting the application of intracavity filters or saturable absorbers. The proposed concept employs a single Tm-doped fibre as the gain medium, saturable absorber and element responsible for filter-less wavelength tuneability simultaneously. Experimental studies show that a ring fibre oscillator comprising such fibre and only a few conventional non-polarisation-maintaining components can support the generation of near transform-limited 350-fs soliton pulses with ~1.2 nJ energy at ~45 MHz repetition rate. Importantly, we explore the impact of Tm^{3+} ion-pair clusters on the saturable absorption properties of doped silica fibres. Moreover, the ultrafast fibre laser system demonstrates effective continuous wavelength tuneability within the range spanning from 1873 to 1962 nm by controlling the cavity feedback and maintaining high quantum efficiency. For this, we suggest employing a variable output coupler, which determines the intracavity energy and, therefore, the excitation level of fibre gain. The rigorous theoretical investigation confirms experimental observations of the pulse formation and clarifies the origin of the tuneability effects.

Overall, the elegance and low complexity of the laser system, together with one order of magnitude shorter pulse duration and more than a twofold increase of the tuneability range are the advancements where we focus the key claims of the current work. Another advantage of the demonstrated technique is that it can be translated to other laser configurations and wavelength ranges, which currently lack an extensive selection of components to develop robust fibre-based systems. The demonstrated technique holds high potential in exploring the Mid-IR range, where rare-earth fibres demonstrate broad gain spectra (e.g. Dy^{3+} ions allow nearly 600 nm tuneability around 3.1 μm[37]).

Results

Investigations of saturable absorption origins in Tm-doped gain fibre. The origin of the saturable absorption in rare-earth-doped fibres is associated with ion pairs excited-state absorption[38–40] and upconversion interaction[41,42]. In the context of Tm-doped fibres, the work of Jackson et al. has concluded that $^3F_4$, $^3F_4 \rightarrow {}^3H_6$, $^3H_4$ (Supplementary Fig. S1a) energy transfer upconversion in unpumped ions plays a key role in establishing the saturable absorption behaviour[43]. The energy difference of this transition is relatively high, $-1500\,cm^{-1}$, and, therefore, a quite high degree of clustering is required for the Tm-doped silica fibres to achieve ion separations that are short enough to provide a sufficient level of saturable absorption.

To reveal the nature of saturable absorption, we examined non-polarisation-maintaining highly Tm-doped fibre with a 2.9 μm core radius, 0.18 numerical aperture and a cut-off wavelength of 1389 nm. The glass matrix of the fibre core comprises an aluminosilicate host with 2.85 mol.% Al_2O_3 and 0.33 mol.% Tm_2O_3, thus providing an 8.6:1 Al:Tm doping ratio. It is worth mentioning that our measurements provided only indicative values of the ion concentration due to the limited resolution of the electron microscope and the small size of the fibre core. Nevertheless, these estimations suggest that the Al concentration is not sufficient to prevent the clustering of Tm ions[44]. A transverse refractive index measurement can be seen together with scanning electron microscope images of the fibre facet in Fig. 1a. Judging from these measurements, the fibre exhibits a pronounced core circularity and concentricity with a characteristic dip in the core centre due to the decrease of Al^{3+} concentration due to the formation of volatile AlF_3[45]. Furthermore, the refractive index profile features are depressed by the F-doping cladding area.

It is worth noting that we also investigated another fibre sample with a germanoaluminosilicate matrix of the core with ~13 mol.% GeO_2, 1.58 mol.% Al_2O_3 and 0.54 mol.% Tm_2O_3, resulting in Ge:Al:Tm ion concentration ratio of 12:3:1 (Supplementary Note 2). However, despite high doping concentration and potential ion clustering, this fibre did not enable self-mode-locking generation in the above-discussed laser configuration. Therefore, further measurements of its properties are presented in Supplementary Materials (Supplementary Fig. S2).

Fluorescence lifetime. The time-resolved luminescence properties, especially the decay time-power dependency, can provide important information about the Tm^{3+} ion incorporation in the optical fibre matrix and the formation of clusters and ion pairs. The fluorescence lifetimes of the $^3F_4$ and $^3H_4$ levels were measured by direct in-band pumping using 1618 and 792 nm diodes. The emission was collected at around 2 μm and 800 nm using InGaAs and Si photodiode detectors, as discussed by Kamrádek et al.[46]. In order to suppress the influence of light travelling along the waveguide, namely the amplified spontaneous emission and reabsorption, the measured fibre was only 1.5 mm long, and the emission was detected transversely. The decay time, τ, was obtained from the e^{-1} value on the normalised decay curve. The fluorescence lifetime, τ_0, was retrieved by extrapolation of the decay time to zero excitation power, assuming the behaviour according to ref. [47]:

$$\tau = \frac{\tau_0}{1 + \left(\frac{\tau_0}{\tau_{sat}} - 1\right)\left(\frac{P}{P + P_{crit}}\right)^2}, \quad (1)$$

wherein τ_{sat} is the saturated lifetime, extrapolated to infinite excitation power, P is the excitation power, and P_{crit} is the critical power of the energy-transfer processes.

Figure 1c shows the lifetime values of the Tm-doped fibre under the study. The value 425 μs of the $^3F_4$ level lifetime is characteristic for highly doped Tm fibres[48]. Importantly, the steep decrease in decay time with increasing excitation power suggests a high rate of energy-transfer upconversion. The experimentally obtained value of $^3H_4$ lifetime is around 21.4 μs, which is also typical for highly doped Tm fibres. Conventionally, the $^3H_4$ decay time of highly doped fibres with homogeneously distributed Tm^{3+} ions should increase with excitation power due triggering the cross-relaxation effect $^3H_4, {}^3H_6 \rightarrow {}^3F_4, {}^3F_4$. As observed in our fibre sample, the decrease of decay time with excitation power suggests a suppressed cross-relaxation and, therefore, further supports the hypothesis of clustering and pair-induced quenching of Tm ions.

Pump saturable absorption. For estimating the concentration of Tm^{3+} pairs in our active fibres, we used the approach proposed by Myslinski et al.[49] for measuring the saturable loss of the pump absorption. Departing from the measurement of the pump absorption coefficient as a function of the irradiated pump power (Fig. 1b), we model the non-saturable loss growing with the fraction of Tm-pairs using RP Fiber Power software.

A 18-cm long section of studied Tm-doped fibre demonstrated a small-signal absorption, α_0, of ~15.3 dB. Towards high irradiation, the experimentally recorded pump absorption coefficients saturate at 2.5 dB, following the trend described as:

$$\alpha_{sat} = mk\alpha_0\left\{1 - \frac{\sigma_a + \sigma_e}{m\sigma_a + \sigma_e}\right\}, \quad (2)$$

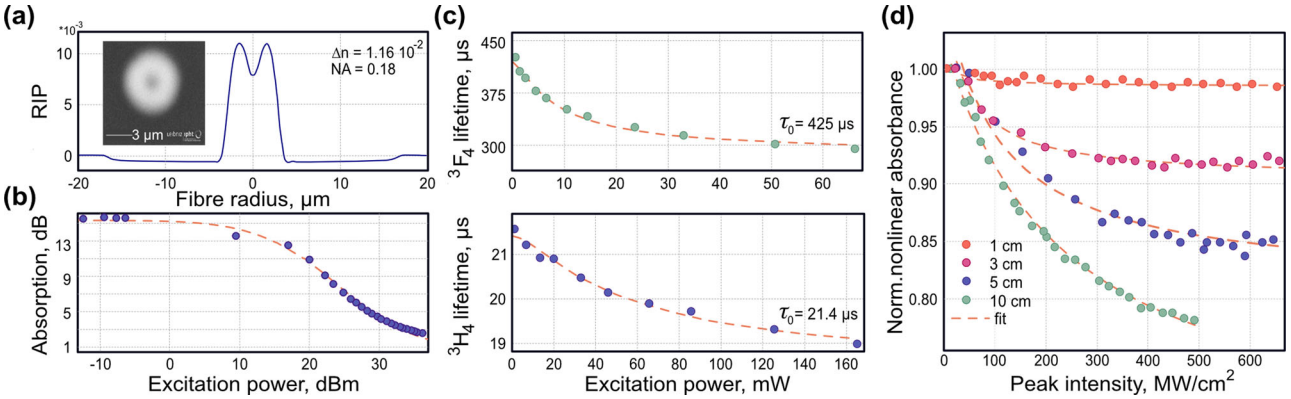

Fig. 1 Tm-doped fibre parameters. a Refractive index profile (RIP). Inset: Scanning electron microscopy image of the fibre core; **b** pump saturable absorption of 18-cm fibre section at 1550 nm. **c** Fluorescent lifetime of the $^3H_4$ and $^3F_4$ manifold against pump power for 1.5-mm fibre length; **d** normalised nonlinear absorption for four length of the Tm-doped fibre.

here k is the proportion of Tm^{3+} clusters in the total Tm^{3+} concentration, m is the number of ions per cluster[50]. To define the model, we used parameters of Tm-doped fibre, recorded during the fluorescence lifetime measurement and the upconversion coefficients from Kamradek et al.[46]. The fibre indicated the significant contribution of upconversion processes to the $^1G_4$ level, corresponding to 480 nm. Since the pump at 1550 nm wavelength could not provide single-photon excitation to the $^1G_4$, our simulation accounted for the multiphoton or cooperative process as a third-order term quenching, which is limited by used RP Fibre Power software. We assumed cubic quenching coefficient of $2.8 \cdot 10^{-73}\,m^3\,s^{-1}$ in the simulations. This third-order quenching coefficient ensured considerably better agreement with experimentally measured data, preventing numerical absorption curves from saturating far too fast at lower launched pump powers (Fig. 1b). The detailed numerical simulation allowed estimation of ~20% of Tm^{3+} pairs in the studied gain fibre.

Nonlinear saturable absorption. To measure the saturable absorption of the active fibre via the twin-detector approach, we used a self-build Tm-doped fibre laser generating 500-fs pulses at 1890 nm. The laser output power, controlled via an external variable optical attenuator, was split into two arms and launched into an unpumped fibre under test and a reference detector. Since the saturable absorption behaviour is considered to occur in unexcited rare rare-earth-doped optical fibre, we investigated nonlinear dynamics at 1, 3, 5 and 10-cm long fibre sections. Figure 1d shows the normalised intensity-dependent absorption measurement data with the approximation according to the two-level energy model[51]:

$$\alpha(I) = \frac{\alpha_0}{1 + \frac{I}{I_{sat}}} + \alpha_{ns}, \quad (3)$$

where α_0 and α_{ns} are the modulation depth and non-saturable losses, correspondingly. I is the launched pulse intensity, and I_{sat} is the saturation intensity, which corresponds to the twice reduced absorption of the test sample. As seen in Fig. 1d, the saturation intensity of Tm-doped fibre drops from 250 to 72 MW cm^{-2} with the reduction of the active fibre length. The active fibre demonstrates high modulation depth spanning from 34 to 9.5%, when trimmed from 10 to 3 cm. These values are comparable with the parameters of conventional material saturable absorbers, operating at SWIR wavelength range[52]. However, the saturation intensity of Tm-doped fibre is significantly higher, which can be explained by a high energy difference between the initial and final upconversion energy states. Moreover, the peak power of the available ultrafast fibre laser was not sufficient to fully saturate the Tm-doped fibre section with the 10-cm length. Therefore, we anticipate that the longer section would not act as an efficient saturable absorber or require considerable laser gain to compensate for the high saturation threshold. Similarly, the decrease of the length to ~1 cm cannot provide benefits to self-mode-locking initiation, as the modulation depth drops to nearly 1% with the saturation intensity on only ~40 MW cm^{-2}.

Further, to assess the influence of laser operation wavelength on saturable absorption of the Tm-doped gain fibre, we have investigated the power-dependent absorption at various wavelengths within the tuneability range from 1880 to 1947 nm. The summary of the saturable absorption parameters of 5-cm long Tm-doped fibre section at 1880, 1900, and 1920 nm wavelengths is presented in Supplementary Fig. S3. It is worth noting that the trend of the measured values of the saturable loss coincides well with the relative absorption slope of Tm^{3+} ions. The saturation intensity depends on the upper state lifetime τ and the absorption cross-section σ_{abs} expressed as $I_{sat} = hc(2\lambda\tau\sigma_{abs})^{-1}$, such that the modulation depth is proportional to the absorption cross-section, taking Supplementary Eq. (S1) into account.

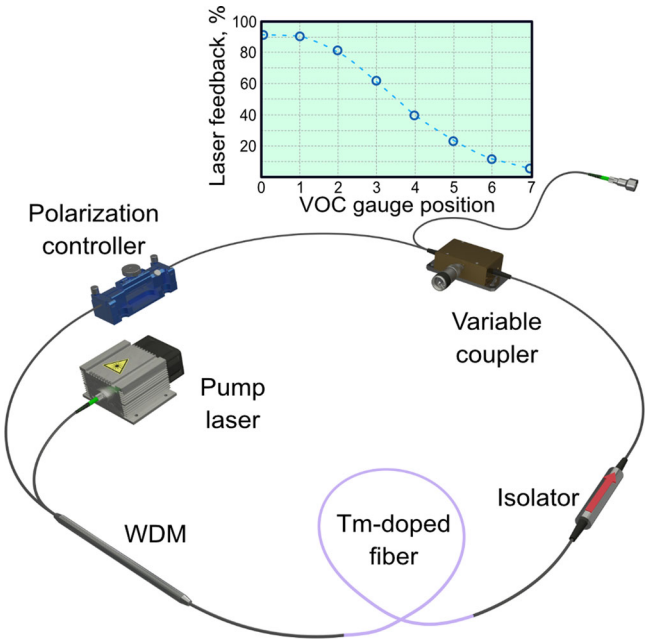

Fig. 2 Schematic of the ultrafast Thulium-doped fibre laser. The oscillator comprises a single-mode pump laser (Er-doped fibre laser at 1.55 μm), a wavelength division multiplexer (WDM), Tm-doped fibre, a polarisation-insensitive isolator, an in-line variable output coupler (VOC) and a squeezing type polarisation controller. All passive fibres are polarisation-insensitive SMF28e. Note, the VOC is replaced by a fixed, fused coupler with 20% feedback for the section "Pulse duration and laser optimisation". The inset depicts the nonlinear course of the coupling coefficient against the VOC's gauge.

Experimental configuration. To examine the self-mode-locking and tuneability dynamics of the ultrashort pulse generation in the laser cavity with a variable Q-factor, we assembled the Tm-doped fibre laser setup as presented schematically in Fig. 2. The ring fibre laser cavity employed a 1550-nm pump laser with 1-W power (HPFL-300, BKtel), a 1550/2000 wavelength division multiplexer, an isotropic isolator, and a squeezing polarisation controller to restore the polarisation state after each round trip. A 0.5 m section of a non-polarisation maintaining Tm-doped silica fibre, discussed in the previous chapter, provided both active gain and saturable absorption to enable self-mode-locking. The fibre small-signal gain was estimated as ~30 dB (for 0.95 W pumping and 65 μW seeding a 44 cm piece). Next, the active fibre group velocity dispersion, third-order dispersion and nonlinearity were estimated as $\beta_2 = -20$ ps^2/km, $\beta_3 = 0.27$ ps^3/km, $\gamma = 2\,W^{-1}\,km^{-1}$, correspondingly, at around 1.9 μm wavelength range. The rest of the cavity comprises 4.2 metres-long standard single-mode fibre ports of the fiberised laser components with the following parameters: $\beta_2 = -59$ ps^2/km, $\beta_3 = 0.28$ ps^3/km, $\gamma = 1.3\,W^{-1}\,km^{-1}$ at Tm-doped fibre laser operation wavelength. It is important to stress that the oscillator consists fully of polarisation-insensitive elements and concentric, cylindrical silica fibres. Therefore, any other mode-locking mechanism, particularly NPE, could be not considered due to short cavity length and negligible polarisation dependent loss[53].

The tuneability of the laser generation was established by introducing no filtering elements into the cavity, but only through including an in-line variable fibre-optic coupler (Evanescent Optics) based on D-shaped polished fibres, interacting via the

evanescence field. The separation of these fibres changes through rotating a knob controller, thus, modifying the coupling efficiency from one waveguide into another, and overall laser cavity feedback from 8 to 93% with nearly 0.3–0.1 dB excess loss. The performance of the variable coupler was characterised by reference laser transmission measurements at 1.95 μm and is shown in the inset in Fig. 2.

Numerical simulations. To validate the possibility of the self-mode-locking and broadband tuneability in the presented Tm-doped fibre laser, we developed a numerical model which describes consequent pulse propagation through different cavity elements. The pulse propagation along the passive fibre is governed by the Nonlinear Schrödinger equation. The following system of coupled equations for continuous-wave pump and pulsed signal generation, taking into account the effects of dispersion and nonlinearity, was considered to describe the signal amplification[54,55]:

$$\frac{\partial A_s(z,t)}{\partial z} = -i\frac{\beta_2}{2}\frac{\partial^2 A_s(z,t)}{\partial t^2} + i\gamma|A_s(z,t)|^2 A_s(z,t) + \int_{-\infty}^{\infty}\frac{g_s(\omega,z)}{2}\tilde{A}_s(z,\omega)\exp(-i\omega t)d\omega, \quad (4)$$

$$\frac{\partial P_p(z)}{\partial z} = g_p(z)P_p(z), \quad (5)$$

where $A_s(z,t)$ is the slowly varying envelope associated with the signal, $P_p(z)$ is the average power of continuous-wave pump, β_2 is the group velocity dispersion, γ is the Kerr nonlinearity, g_s and g_p are signal and pump gain/loss coefficients, correspondingly. Equation (4) was numerically solved by the split-step Fourier method. The spectral window considered in the model extended from 1300 to 2800 nm. The temporal window was equal to 140 ps.

The wavelength dependence of the gain is considered in the frequency domain, where optical field $\tilde{A}(z,\omega)$ is multiplied by the gain profile $g_s(\omega,z)$. Each spectral component of the gain $g_s(\lambda_i,z)$ ($i=1,..,N_\omega$, where N_ω is the number of the discrete frequencies in simulations) and pump gain/loss coefficient at each step along the fibre were found from the rate equations in the stationary case $dN_{2,3}/dt=0$:

$$g_s(\lambda_i,z) = \left(\sigma^s_{21}(\lambda_i)-\sigma^s_{23}(\lambda_i)\right)\rho_s(\lambda_i)N_2(z) - \sigma^s_{12}(\lambda_i)\rho_s(\lambda_i)N_1(z) + \sigma^s_{32}(\lambda_i)\rho_s(\lambda_i)N_3(z),\ i=1,\ldots,N_\omega \quad (6)$$

$$g_p(z) = \sigma^p_{21}\rho_p N_2(z) - \sigma^p_{12}\rho_p N_1(z), \quad (7)$$

$$\frac{dN_2(z)}{dt} = \left(\sigma^p_{12}\rho_p\frac{P_p(z)}{h\nu_p} + \sum_{k=1}^{k}\left(\sigma^s_{12}(\lambda_k)\rho_s(\lambda_k)\frac{P_s(\lambda_k,z)}{h\nu_k}\right)\right)N_1(z) + \left(\sum_{k=1}^{k}\left(\sigma^s_{32}(\lambda_k)\rho_s(\lambda_k)\frac{P_s(\lambda_k,z)}{h\nu_k}\right)\right)N_3(z) - \left(\sigma^p_{21}\rho_p\frac{P_p(z)}{h\nu_p} + \sum_{k=1}^{k}\left(\sigma^s_{21}(\lambda_k)\rho_s(\lambda_k)\frac{P_s(\lambda_k,z)}{h\nu_k}\right) + \sum_{k=1}^{k}\left(\sigma^s_{23}(\lambda_k)\rho_s(\lambda_k)\frac{P_s(\lambda_k,z)}{h\nu_k}\right) + \frac{1}{T_2}\right)N_2(z) - 2k_{2231}N_2^2 + 2k_{3122}N_1N_3,$$

$$\frac{dN_3(z)}{dt} = \left(\sum_{k=1}^{k}\left(\sigma^s_{23}(\lambda_k)\rho_s(\lambda_k)\frac{P_s(\lambda_k,z)}{h\nu_k}\right)\right)N_2(z) - \left(\sum_{k=1}^{k}\left(\sigma^s_{32}(\lambda_k)\rho_s(\lambda_k)\frac{P_s(\lambda_k,z)}{h\nu_k}\right) + \frac{1}{T_3}\right)N_3(z) + k_{2231}N_2^2 - k_{3122}N_1N_3, \quad (8)$$

$$N_1(z) = N - N_2(z) - N_3(z), \quad (9)$$

here $N_{1,2,3}$ are population densities in the energy levels $^3H_6$, $^3F_4$ and $^3H_4$ correspondingly, $N=4.05938\cdot10^{15}\,m^{-1}$ is the total number of Tm-ions integrated over the fibre mode cross-section, $P_s(\omega_k,z)=|\tilde{A}(z,\omega_k)|^2$ is the signal power at the frequency ω_k and position z along the fibre, $T_2=425\,\mu s$ and $T_3=21.4\,\mu s$ are fluorescence lifetimes. The effective pump absorption and emission cross-sections at pump wavelengths are $\sigma^p_{12}=1.5630\cdot10^{-25}\,m^2$ and $\sigma^p_{21}=5.1005\cdot10^{-27}\,m^2$. The absorption and emission cross-section spectra in the considered spectral window (shown in Supplementary Fig. S4) are described by $\sigma^s_{12}(\lambda_i)$, $\sigma^s_{23}(\lambda_i)$, $\sigma^s_{21}(\lambda_i)$ and $\sigma^s_{32}(\lambda_i)$. The normalised pump and signal power distributions through the fibre cross-section are marked $\rho_{p,s}=\Gamma_{p,s}/\pi a^2$, where $a=2.65\,\mu m$ is the core radius of a single-mode fibre, $\Gamma_p(\Gamma_s)$ corresponds to the modal overlap factor between the pump (signal) mode and the ion distribution. $\Gamma_p=1$ for core pumping, $\Gamma_s=1-\exp(-2a^2/w^2)$, w is 1/e electric field radius of the equivalent Gaussian spot. The energy transfer coefficients $k_{3122}=2.52\cdot10^{-22}\,m^3/s$ and $k_{2231}=3.44\cdot10^{-24}\,m^3/s$ describe the cross-relaxation process $^3H_4$, $^3H_6\rightarrow{}^3F_4$, $^3F_4$ and energy transfer upconversion $^3F_4$, $^3F_4\rightarrow{}^3H_4$, $^3H_6$ correspondingly[48].

The used approach $dN_i/dt=0$ means that this evolution occurs with the roundtrips quite slowly, i.e., during one round trip the optical field does not change the populations N_1, N_2, N_3 significantly. At the end of the active fibre, the pump is depleted, and the last fibre segment plays the role of a saturable absorber. Equations (4)–(9) are also applicable to describe the optical losses ($\alpha=-g_s$) experienced by the signal beam in the absence of the pump power. In this case, the condition $dN_i/dt=0$ sets an instantaneous response of the saturable absorber on the pulse power within each round-trip. It results in the non-saturated losses α_{ns} determined by the ion quenching and up convention processes and the saturated absorption fraction (Eq. (3)), expressed through the modulation depth α_0, saturation intensity I_{sat} and with $I(t)=|A(t)|^2$. Specifically, for our numerical simulations, we have simplified the model considering the active fibre as a combination of the amplifier described by the wavelength-dependent gain profile $g_s(\lambda_i,z)$ distributed over the whole fibre length and an absorber described as the time-dependent optical losses $\alpha(t,z)=-g_s(t,z)$ localised in a rare end of fibre section. Such consideration has allowed us to separate contributions of the amplification and saturable absorption to the laser dynamics and utilise for simulations the characteristics of Tm-doped fibre directly measured in the experiment (Fig. 1d). In fact, an analogous approach based on a combination of the wavelength-dependent and time-dependent gain has been recently applied for accurate modelling of optical pulse propagation in Yb-doped fibres[56]. However, the used gain presentation as a product of wavelength-dependent and time-dependent factors was rather artificial to approximate a more complicated mathematical function.

The initial field at the first round trip was modelled with "white" Gaussian noise. As Fig. 3a illustrates, a lasing self-start could not be obtained using saturable absorber with saturation intensity $I_{sat}=46\,MW/cm^2$, corresponding to the shortest 1-cm long fibre samples. The optical field tends to zero in this case. The optimal value of saturation intensity is $I_{sat}=150\,MW/cm^2$, which match the parameters of 5-cm section of Tm-fibre used in the experiments. Here, we observed the formation of stable pulse generation (Fig. 3b). Further increase of saturation intensity leads to the distortion of the pulse, significant growth of the Kelly sidebands (Fig. 3c) and pulse break-up (Fig. 3d). Therefore, in further simulations, we fixed parameters of saturable absorber at values corresponding to 5-cm long Tm-doped fibre saturable absorber, i.e. $\alpha_0=0.15$ and $\alpha_{ns}=0.85$, $P_{sat}=100\,W$.

Figure 4a shows simulated output spectra at different gain excitation levels. The increase in cavity feedback leads to a red-

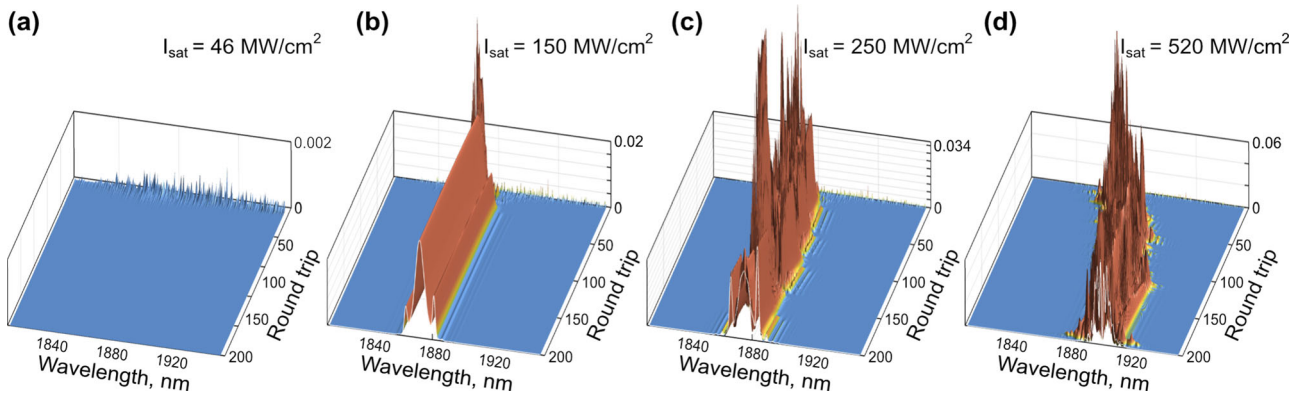

Fig. 3 Theoretical simulation of spectral evolution during pulse formation with variable saturable absorber properties. The first 200 round trip of the pulse formation are evaluated in a spectral domain. For **a**–**d** increasing values of the Tm-doped fibre saturation intensity (I_{sat}) is assumed from 46 to 52 MW/cm^2. Vertical axis corresponds to normalised intensity (in arb. units).

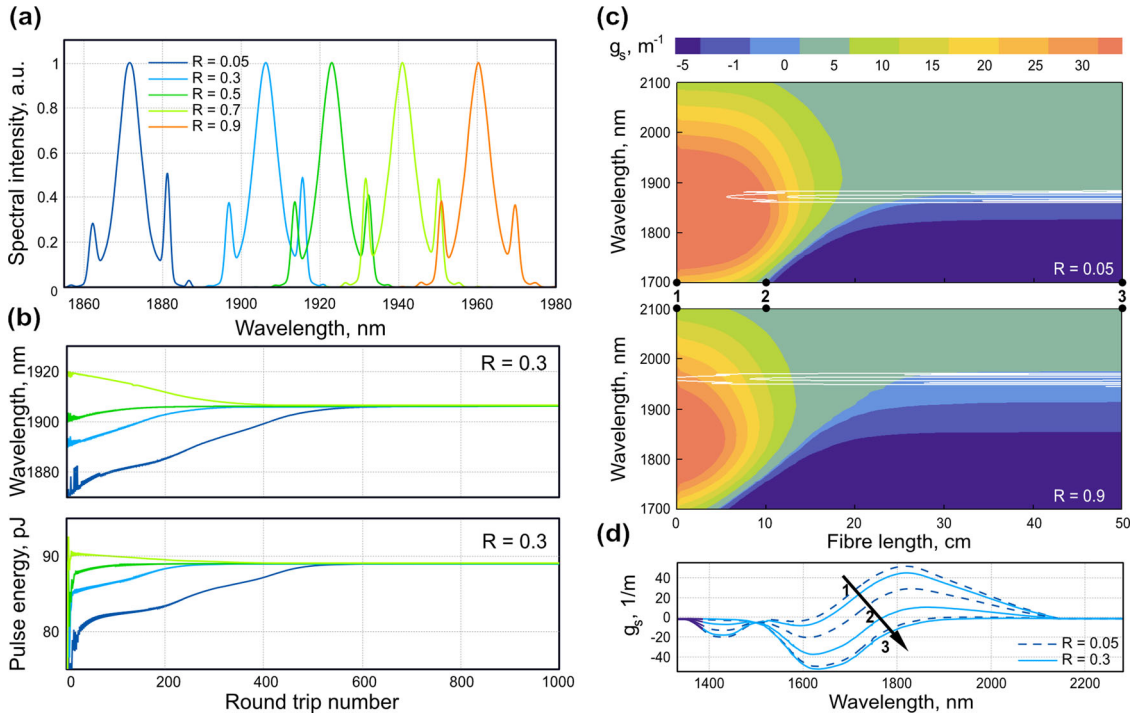

Fig. 4 Numerical simulations results of pulse tuneability. a Calculated output spectra corresponding to varying cavity feedback $R = 0.05$–0.9; **b** convergence to steady-state regime of pulse generation from different seed parameters in simulations; **c** evolution of the gain profile along amplifier for $R = 0.05$ (i) and $R = 0.9$ (ii). Insets: white lines depict the pulse spectrum; **d** gain spectra at different points ("1", "2" and "3") along the fibre at 5 and 90% cavity feedback.

shift of the pulse central wavelength from 1872 to 1961 nm, resulting in wavelength tuneability of about 90 nm. The output spectra have pronounced Kelly sidebands characteristic to periodically amplified average solitons.

We also investigated field evolution towards the steady-state mode-locking regime using initial seed pulse with different parameters to confirm the reproducibility and uniqueness of solution. First, a hyperbolic secant pulse with 1.13 pJ energy, 1 W peak power, 1 ps duration and varying wavelength was used as a seed. The simulation results show that the output pulse wavelength and energy in the stable regime do not depend on the wavelength and character of energy evolution of the seed pulse. Figure 4b shows the example of simulation with the feedback ratio of 30%, where four initial pulses with different wavelengths converge to the same attractor with the increase of the cavity round trips number. Different colours of the lines in Fig. 4b correspond to different wavelengths of the seed pulses at the fixed ~1 pJ initial energy. Such dynamics verifies the uniqueness of the steady-state solution. Overall, this study justifies that the tuneability of the central operation wavelength in the filter-less laser cavity under investigation is governed solely by the wavelength-dependent gain distributed over the fibre length.

To better understand the nature of the tuneability dynamics, we considered the evolution of the gain $g_s(\lambda)$ along the active fibre corresponding to the cavity feedback values $R = 5\%$ and $R = 90\%$ (Fig. 4c). The pulse spectrum in steady-state is depicted by white lines in Fig. 4c. A feedback increase from 5 to 90% leads to higher pulse energy inside the cavity and faster gain saturation. The gain maximum shifts towards a higher wavelength and causes the shift

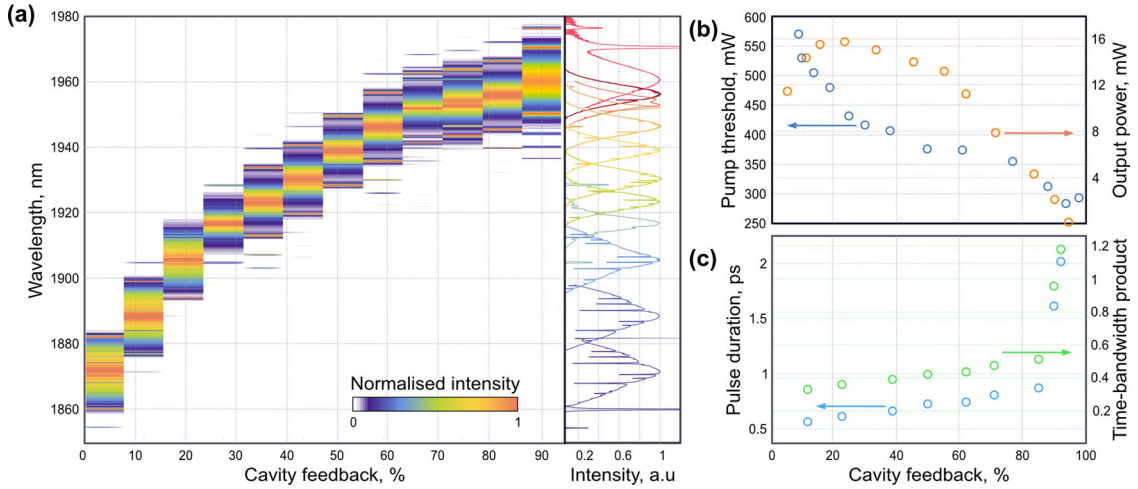

Fig. 5 Experimental study of feedback-controlled laser tuneability. Variation of output pulse characteristics with the variable coupler providing 8 to 93% feedback at fixed polarisation state and 0.7 W pump power. **a** Wavelength tuneability of the optical spectrum; **b** variance of the pump threshold (blue, left axis) and output power (orange, right axis); **c** alteration of pulse duration (blue, left axis) and time-bandwidth product (green, right axis).

of the pulse spectrum to find energy balance. Thus, absorption and amplification actively reshape the gain spectrum along the fibre, driving the pulse wavelength. Gain spectra measured at the points "1", "2", and "3" along the fibre (Fig. 4d) qualitatively agree with the spectra shown in Supplementary Fig. S1.

The system of the coupled Eqs. (4)–(9) allows to describe amplification of a narrow sub-picosecond pulse accompanied by dynamically evolving gain spectrum. Note, that in the conventional approach for modelling of Tm-doped amplifiers the system of population inversion rate equations is written for the continuous-wave signal and pump and describes evolution of the average powers[43,46,48]. The spectral dependence of the gain and nonlinear pulse propagation along the fibre are not taken into account. Here we solve the population inversion rate equations simultaneously with the pulse evolution, where spectral dependence of the gain is calculated at each step along the fibre. Therefore, wavelength tuneability of the output pulse can be demonstrated.

Experimental laser characterisation. We next examined the self-mode-locked Tm-doped fibre laser experimentally. The application of 50 cm of Tm-doped fibre in the ring laser cavity allowed achieving stable self-starting ultrashort pulse generation. Notably, the self-mode-locked operation was observed within the entire range of the cavity feedback tuneability from 8 to 93%, yet featured a different threshold. In general, the mode-locking threshold was relatively higher than one for the schemes with conventional material saturable absorbers. This can be explained by the high saturation intensity (Fig. 1d) of Tm- doped fibre when it acts as a saturable absorber. In contrast to conventional ultrafast lasers, the efficiency of the mode-locked regime is lower than that of continuous-wave generation. We attribute this to the nature of the saturable absorption mechanism in Tm-doped fibre associated with the reabsorption of the laser signal. The intracavity polarisation controller required proper initial adjustment, while later, after several switching on-off cycles, the self-mode-locking regime could self-start without polarisation tuning.

The continuous central wavelength tuneability of the self-mode-locked generation was observed in the range spanning from 1873 and 1962 nm (Fig. 5a) without further alignment. As the numerical simulation predicted, the tuneability was highly reproducible with the feedback variation even after several switch-on and off cycles. Here, we would like to stress that to investigate tuneability dynamics of the single-pulse generation under the same conditions, the pump power and polarisation state in the cavity were fixed, while only the feedback was altered. Naturally, at higher feedback, hence, higher intracavity energy, the fundamental soliton generation regime tended to break into multi-pulsing with the pump power increase. Therefore, we limited the pump power at 0.7 W. Supplementary Movie 1 demonstrates smooth wavelength tuneability of the self-mode-locked generation with no pulse break up or instabilities. The variation of output average power at 0.7 W pump power is presented in Fig. 5b (blue scatters). Its trend is in good agreement with the laser efficiency dynamics predicted numerically using the Rigrod model[57] (Supplementary Fig. S5), which showed the highest efficiency at 20% cavity feedback. While the efficiency is decreasing for longer laser operation wavelengths, this deterioration can be efficiently mitigated by appropriate optimisation of background losses according to Rigrod analysis.

Figure 5b, c demonstrates self-mode-locked pulse parameters at the laser output with the different outcoupling ratio. Thus, the pulse duration broadened from 550 to 860 fs with the feedback increase. At the same time, the spectral full width at half-maximum ranges only from 7.4 to 7.7 nm with the increase of the cavity feedback. Consequently, the pulses evolve from nearly transform-limited below 12% cavity feedback to slightly chirped with decreased outcoupling. At high feedback values (over 85%) and, therefore, high intracavity intensities, the time-bandwidth product rises to 1.172, indicating that nonlinear effects do not balance the cavity dispersion. With the increase in feedback, the pump power threshold for achieving self-mode-locking decreased from 538 to 289 mW (Fig. 5b). At the same time, the upper threshold for stable single-pulse operation reduces with higher feedback due to gain saturation.

With careful adjustment of the polarisation controller, the maximum average output power of 68 mW could be obtained in a single-pulse generation regime with 25% feedback and maximum available pump power of 1240 mW, resulting in 5.5% optical conversion efficiency. It is important to notice that neither saturation of the output power nor degradation of any components were observed, while the only limitation for further power increase was the availability of a pump source. Figure 6 demonstrates the output pulse parameters at the highest average power. With its central wavelength at 1889 nm, the optical spectrum displays a bandwidth of 6.8 nm with pronounced Kelly-sidebands, as depicted in Fig. 6a. Figure 6b demonstrates an autocorrelation trace with $sech^2$ approximation and full width at

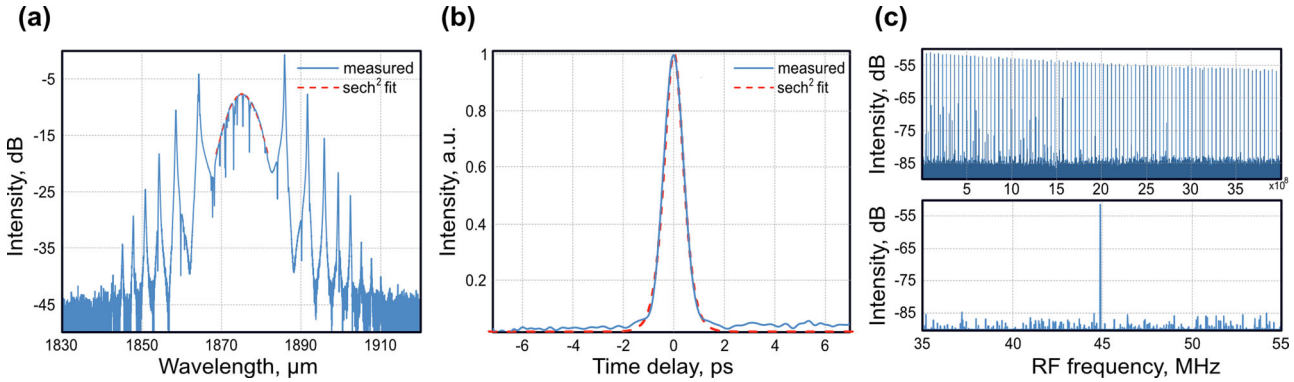

Fig. 6 Measured output pulse characteristics with highest average power. a Optical spectrum centred at 1889 nm; **b** autocorrelation trace with *sech*^{2} fit; **c** RF spectrum over 40 GHz (i) and a close-up of the fundamental frequency (ii).

half-maximum of ~870 fs, resulting in a soliton pulse duration of ~600 fs. The fundamental repetition rate complies with the fibre laser cavity length at around 44 MHz (Fig. 6c). Note that the RF spectrum was retrieved numerically via the fast Fourier transform of the pulse train, recorded by the oscilloscope with the dynamic range of 5.5 bits. This limited the signal-to-noise ratio to ~34 dB. Overall, it yields a peak power of 1.6 kW, corresponding to 1.0 nJ pulse energy, bearing in mind that nearly 26% of the total power belongs to the sidebands.

Furthermore, the self-mode-locked generation regime can be adapted by using the feedback variation. Supplementary Fig. S6 shows the map of possible generation regimes with fixed polarisation controller and with its adjustment, ensuring single-pulse generation when possible. The laser regime can be switched from the generation of fundamental solitons to soliton complexes, stable high-harmonics generation (up to fourth order), and chaotic behaviour.

Pulse duration and laser optimisation. As we mentioned before, the self-mode-locking dynamics rely on the fibre cavity nonlinearity, being assisted by SPM. To validate this fact, we have replaced the tuneable coupler in the laser cavity with a fused one, enabling 20% cavity feedback as predicted by Rigrod analysis (Supplementary Fig. S5). In this case, the maximum output power reached 83 mW at 903 mW pump power, resulting in the laser slope efficiency of 14.5%. The output autocorrelation trace, spectrum and pulse train are shown in Supplementary Fig. S7. In brief, the output optical spectrum is centred at 1888 nm. The intensity autocorrelation features a symmetric *sech*^{2} peak without secondary signals or a substantial pedestal, which estimates the pulse duration of 350 fs. We tested the self-mode-locked Tm-doped fibre laser generation at maximum output performance over 49 h of continuous operation to confirm its stability. Supplementary Fig. S7d justifies that no pulse breakup occurred, merely a negligible variance in the intensity of sidebands and ~1 nm the central wavelength blue-shift due to temperature fluctuations in the laboratory.

To get a deeper insight into the saturable absorption performance of the Tm-doped fibre and separate this role from the one of the gain medium, we studied the self-mode-locking regime while gradually cutting back the length of the active fibre. Our findings demonstrate that the mode-locking dynamics are sensitive to the length of the active fibre. In the experiments, the ultrashort pulse generation could still be achieved with the length of Tm-doped fibre reduced from 50 down to 47.8 cm with the fine-tuning of the polarisation controller. However, Q-switch intensity modulation became more pronounced and affected the quality of the generation. The cut-back studies demonstrated a reduction of the spectral bandwidth of the generated solitons down to 0.95 nm, as shown in Supplementary Fig. S8. It also reveals the rise of the mode-locking threshold from 610 mW pump power at the original length, over 690–810 mW. In addition, laser efficiency increased with the active fibre length reduction, which can be explained by reduced losses due to signal reabsorption in the unexcited rear part of the active fibre. Overall, the experimental studies supported by numerical simulations presented in Fig. 3 allow us to conclude that only a rear unexcited section of Tm-doped fibre (with a length of around 5–7 cm) can efficiently operate as a saturable absorber.

Discussion

Our comprehensive investigation of highly Tm-doped fibre properties has confirmed that highly Tm-doped fibre can efficiently operate as a laser gain and saturable absorber and provide generation wavelength tuneability. While comparing two fibre samples with different core glass matrixes and comparable Tm concentrations, we concluded that the refractive index profile is not a decisive criterion for fibre performance as a saturable absorber. In contrast, the important aspects for saturable absorption are the strongly quenched lifetime for the $^3F_4$ level, a rather low cross-relaxation action for the $^3H_4$ level and certain concentration of Tm^{3+} pairs. These features justify reinforced interionic energy transfer mechanisms between $^3F_4 \rightharpoonup {}^3H_6$: $^3H_6 \rightharpoonup {}^3F_4$ levels. Our study confirms that the estimated concentration of Tm^{3+} ion pairs of 20% equips aluminosilicate gain fibre with 23% modulation depth and high saturation intensity (95 MW cm^{-2}). These parameters appeared to be sufficient for establishing effective self-mode-locking generation. On the other hand, the germanoaluminosilicate Tm-doped fibre demonstrated a more complicated quenching of Tm ions, and our measurements did not confirm the presence of ion pairs. This fibre featured excessively high saturation intensity and could not initiate mode-locked generation in our laser configuration. Nevertheless, detailed spectroscopic and pump-probe investigation of various Thulium-doped fibre compositions would be beneficial for in-depth evaluation of the impact of clustering and quenching processes on the relaxation and saturable absorption behaviour.

Furthermore, the presented experimental and numerical studies of the self-mode-locked Tm-doped fibre laser with variable feedback demonstrated broadband central wavelength tuneability. The results of numerical simulations agree well with the experiment, demonstrating the same tuneability range. Both investigations have confirmed the variation of the gain excitation level through alteration of cavity feedback to be the primary mechanism of the tuneability of the ultrashort pulse spectrum. Our numerical simulations have also confirmed that the range of

observed gain-controlled tuneability through laser feedback variation is determined by the emission cross-section and bandwidth of used Tm-doped fibre (see Supplementary Fig. S4). It is important to note that the amplification and absorption, responsible for different aspects of the laser dynamics, are localised in different parts of the fibre. Wavelength tuneability is provided by wavelength-dependent gain distributed over the fibre length, whereas the saturable absorption localised at the fibre rear end is responsible for the pulse formation.

In conclusion, the experimental and theoretical investigations reported in the current work have extended the understanding of gain dynamics in ultrafast fibre lasers. The self-mode-locked laser setup enabled the generation of stable self-starting ultrashort pulses with the duration of 350 fs at 45 MHz repetition rate delivering ~1.2 nJ of the energy in the main pulse peak. To the best of our knowledge, this is the first demonstration of femtosecond pulse generation directly from the self-mode-locked Thulium-doped fibre laser. Moreover, through the alteration of cavity feedback in the ultrafast Tm-doped fibre laser, we have recorded a central wavelength shift within the range spanning from 1873 to 1962 nm. The control of the excitation level and gain through variation of out-coupled power proved to be more advantageous than loss management. Together with a broad emission spectrum and high cross-section, this became enabling aspects for more than doubled tuneability range. From an instrument development viewpoint, our results have provided a further example of the incredible flexibility of ultrafast fibre lasers. The next step to provide a higher stability and avoid polarisation instabilities could be a realisation of all-polarisation maintaining laser cavity employing the concept of feedback-controlled self-mode-locking. Yet, this would require first and foremost the development of a Tm-doped fibre with properties similar and, particularly, glass matrix to the one studied here. Although the current studies were focused on Tm-doped fibres as the gain medium, the key underlying phenomenon of the suggested tuneability method is versatile. It could be translated to other wavelengths, where the majority of fibreised laser components, including filters, are currently unavailable. In particular, this refers to exploring the Mid-IR wavelength range, where Dy and Er-doped fluoride-based fibres also offer exceptionally broad gain spectra.

Methods

Instrumentation. The measuring equipment is made up of a 10 GHz extended InGaAs photodetector (ET-5000, EOT) next to a 25 GS/s oscilloscope (DPO 70604C, Tektronix) for electric characterisation. For optical characterisation an optical spectrum analyser with down to 50 pm resolution and a 1.1–2.5 μm spectral coverage is used (AQ6375, Yokogawa). With a frequency doubling autocorrelator (PulseCheck, APE), the time dependence has been examined. For quantifying the mean optical power, an integrating sphere type sensor with InGaAs photodiode and 1 nW resolution is employed (S148C, Thorlabs).

Data availability

Experimental data underlying the results presented in this paper are available in ref. [58].

Code availability

Computer code for the numerical simulations is available upon reasonable request from the authors.

Received: 8 March 2022; Accepted: 1 August 2022;
Published online: 03 September 2022

References

1. Moro, S., Danicic, A., Alic, N., Usechak, N. G. & Radic, S. Widely-tunable parametric short-wave infrared transmitter for co 2 trace detection. *Opt. Express* **19**, 8173–8178 (2011).
2. Astrauskas, I., Považay, B., Baltuška, A. & Pugžlys, A. Influence of 2.09-μm pulse duration on through-silicon laser ablation of thin metal coatings. *Opt. Laser Technol.* **133**, 106535 (2021).
3. Liang, H., Lange, R., Peric, B. & Spring, M. Optimum spectral window for imaging of art with optical coherence tomography. *Appl. Phys. B* **111**, 589–602 (2013).
4. Xu, C. & Wise, F. Recent advances in fibre lasers for nonlinear microscopy. *Nat. Photon.* **7**, 875–882 (2013).
5. Lin, P. et al. 2-μm free-space data transmission based on an actively mode-locked holmium-doped fiber laser. *IEEE Photon. Technol. Lett.* **32**, 223–226 (2020).
6. Keller, U. et al. Semiconductor saturable absorber mirrors (SESAM's) for femtosecond to nanosecond pulse generation in solid-state lasers. *IEEE J. Sel. Top. Quantum Electron.* **2**, 435–453 (1996).
7. Martinez, A. & Sun, Z. Nanotube and graphene saturable absorbers for fibre lasers. *Nat. Photon.* **7**, 842–845 (2013).
8. Liu, X., Gao, Q., Zheng, Y., Mao, D. & Zhao, J. Recent progress of pulsed fiber lasers based on transition-metal dichalcogenides and black phosphorus saturable absorbers. *Nanophotonics* **9**, 2215–2231 (2020).
9. Wang, Z. et al. Mxene photonic devices for near-infrared to mid-infrared ultrashort pulse generation. *ACS Appl. Nano Mater.* **3**, 3513–3522 (2020).
10. Haus, H., Ippen, E. & Tamura, K. Additive-pulse modelocking in fiber lasers. *IEEE J. Quantum Electron.* **30**, 200–208 (1994).
11. Winful, H. G. & Walton, D. T. Passive mode locking through nonlinear coupling in a dual-core fiber laser. *Opt. Lett.* **17**, 1688–1690 (1992).
12. Zhang, J. et al. Intermode beating mode-locking: toward compact 2 μm short-pulse all-fiber lasers. *Opt. Fiber Technol.* **58**, 102253 (2020).
13. Fontana, F., Begotti, M., Pessina, E. & Lugiato, L. Maxwell-Bloch modelocking instabilities in erbium-doped fiber lasers. *Opt. Commun.* **114**, 89–94 (1995).
14. Xu, C. et al. L-band compact Q-switched fiber laser based on thulium-doped fiber saturable absorber. *Appl. Opt.* **60**, 6843–6848 (2021).
15. Gene, J., Kim, S. K. & Do Lim, S. Validity analysis of holmium-doped fiber as saturable absorber for passively Q-switched thulium-doped fiber laser. *J. Lightwave Technol.* **36**, 2183–2187 (2018).
16. Paschotta, R. & Keller, U. Passive mode locking with slow saturable absorbers. *Appl. Phys. B* **73**, 653–662 (2001).
17. Qamar, F. Z. & King, T. A. Self-mode-locking effects in heavily doped single-clad Tm3+-doped silica fibre lasers. *J. Mod. Opt.* **52**, 1053–1063 (2005).
18. Tsao, H.-X., Chang, C.-H., Lin, S.-T., Sheu, J.-K. & Tsai, T.-Y. Passively gain-switched and self mode-locked thulium fiber laser at 1950 nm. *Opt. Laser Technol.* **56**, 354–357 (2014).
19. Wang, M., Zhao, J., Li, Y. & Ruan, S. Generation of pulse bundles in a self-mode-locked Tm-doped double-clad fiber laser. *Optik* **154**, 485–490 (2018).
20. Dai, R. et al. Nanotube mode-locked, wavelength and pulsewidth tunable Thulium fiber laser. *Opt. Express* **27**, 3518–3527 (2019).
21. Noronen, T., Okhotnikov, O. & Gumenyuk, R. Electronically tunable thulium-holmium mode-locked fiber laser for the 1700-1800 nm wavelength band. *Opt. Express* **24**, 14703–14708 (2016).
22. Liu, F. et al. Tandem-pumped, tunable thulium-doped fiber laser in 2.1 μm wavelength region. *Opt. Express* **27**, 8283–8290 (2019).
23. Sabra, M. et al. Widely tunable dual-wavelength fiber laser in the 2 μm wavelength range. *J. Lightwave Technol.* **37**, 2307–2310 (2019).
24. Vallee, J.-M. et al. Widely tunable silicon-fiber laser at 2 μm. *Opt. Lett.* **46**, 4964–4967 (2021).
25. Sidorenko, P., Fu, W. & Wise, F. Nonlinear ultrafast fiber amplifiers beyond the gain-narrowing limit. *Optica* **6**, 1328–1333 (2019).
26. Bednyakova, A., Kuprikov, E., Geraseva, I. & Kokhanovskiy, A. Influence of spectral filtration on pulse dynamics in ring-cavity Mamyshev oscillator. *Appl. Sci.* **11**, 10398 (2021).
27. Tarasov, N., Perego, A. M., Churkin, D. V., Staliunas, K. & Turitsyn, S. K. Mode-locking via dissipative Faraday instability. *Nat. Commun.* **7**, 1–5 (2016).
28. Chen, S. et al. All-fiber short-wavelength tunable mode-locked fiber laser using normal dispersion thulium-doped fiber. *Opt. Express* **28**, 17570–17580 (2020).
29. Engelbrecht, M., Haxsen, F., Wandt, D. & Kracht, D. Wavelength resolved intracavity measurement of the cross sections of a Tm-doped fiber. *Opt. Express* **16**, 1610–1615 (2008).
30. Chen, S. et al. Ultra-short wavelength operation of thulium-doped fiber amplifiers and lasers. *Opt. Express* **27**, 36699–36707 (2019).
31. Franco, P., Midrio, M., Tozzato, A., Romagnoli, M. & Fontana, F. Characterization and optimization criteria for filterless erbium-doped fiber lasers. *JOSA B* **11**, 1090–1097 (1994).
32. Ghosh, A., Roy, A. S., Chowdhury, S. D., Sen, R. & Pal, A. All-fiber tunable ring laser source near 2 μm designed for CO_2 sensing. *Sens. Actuators B Chem.* **235**, 547–553 (2016).
33. Anjali, P., Sharma, K., Kumar, S., Srinivasan, B. & Venkitesh, D. Demonstration of filterless and tunable thulium doped fiber ring laser with emission in the 2μm region. In *International Conference on Fibre Optics and Photonics*, Tu4A-20 (Optical Society of America, 2016).

34. Harun, S. W., Chong, W. Y., Subramaniam, T. & Ahmad, H. Effect of output coupling reflectivity on performance of l-band erbium-doped fiber laser. *J. Opt. Commun.* **27**, 8–10 (2006).
35. Tarka, J. et al. Power scaling of an all-PM fiber Er-doped mode-locked laser based on graphene saturable absorber. *IEEE J. Sel. Top. Quantum Electron.* **23**, 60–65 (2016).
36. Lin, G.-R., Chang, J.-Y., Liao, Y.-S. & Lu, H.-H. L-band erbium-doped fiber laser with coupling-ratio controlled wavelength tunability. *Opt. Express* **14**, 9743–9749 (2006).
37. Majewski, M. R., Woodward, R. I. & Jackson, S. D. Dysprosium-doped ZBLAN fiber laser tunable from 2.8 μm to 3.4 μm, pumped at 1.7 μm. *Opt. Lett.* **43**, 971–974 (2018).
38. Le Boudec, P. et al. Influence of ion pairs on the dynamical behaviour of er 3+-doped fibre lasers. *Opt. Quantum Electron.* **25**, 501–507 (1993).
39. El-Sherif, A. F. & King, T. A. Dynamics and self-pulsing effects in Tm3+-doped silica fibre lasers. *Opt. Commun.* **208**, 381–389 (2002).
40. Tang, Y. & Xu, J. Model and characteristics of self-pulsing in Tm^{3+}-doped silica fiber lasers. *IEEE J. Quantum Electron.* **47**, 165–171 (2011).
41. Sanchez, F., Le Boudec, P., Francois, P.-L. & Stephan, G. Effects of ion pairs on the dynamics of erbium-doped fiber lasers. *Phys. Rev. A* **48**, 2220 (1993).
42. Colin, S., Contesse, E., Le Boudec, P., Stephan, G. & Sanchez, F. Evidence of a saturable-absorption effect in heavily erbium-doped fibers. *Opt. Lett.* **21**, 1987–1989 (1996).
43. Jackson, S. D. & King, T. A. Dynamics of the output of heavily Tm-doped double-clad silica fiber lasers. *JOSA B* **16**, 2178–2188 (1999).
44. Sincore, A., Bradford, J. D., Cook, J., Shah, L. & Richardson, M. C. High average power thulium-doped silica fiber lasers: review of systems and concepts. *IEEE J. Sel. Top. Quantum Electron.* **24**, 1–8 (2017).
45. Abramov, A. et al. Fabrication of active fluoroaluminosilicate fibers for high-power fiber lasers. *Inorg. Mater.* **54**, 271–275 (2018).
46. Kamrádek, M. et al. Energy transfer coefficients in thulium-doped silica fibers. *Opt. Mater. Express* **11**, 1805–1814 (2021).
47. Vařák, P. et al. Heat treatment and fiber drawing effect on the luminescence properties of RE-doped optical fibers (RE= Yb, Tm, Ho). *Opt. Express* **30**, 10050–10062 (2022).
48. Cajzl, J. et al. Thulium-doped silica fibers with enhanced fluorescence lifetime and their application in ultrafast fiber lasers. *Fibers* **6**, 66 (2018).
49. Myslinski, P., Nguyen, D. & Chrostowski, J. Effects of concentration on the performance of erbium-doped fiber amplifiers. *J. Lightwave Technol.* **15**, 112–120 (1997).
50. Myslinski, P., Chrostowski, J., Koningstein, J. & Simpson, J. R. Self-mode locking in a Q-switched erbium-doped fiber laser. *Appl. Opt.* **32**, 286–290 (1993).
51. Silfvast, W. T. *Laser Fundamentals* (Cambridge University Press, 2004).
52. Kirsch, D. et al. Short-wave IR ultrafast fiber laser systems: current challenges and prospective applications. *J. Appl. Phys.* **128**, 180906 (2020).
53. Jung, M. et al. Mode-locked pulse generation from an all-fiberized, Tm-Ho-codoped fiber laser incorporating a graphene oxide-deposited side-polished fiber. *Opt. Express* **21**, 20062–20072 (2013).
54. Turitsyn, S. K. et al. Modeling of CW Yb-doped fiber lasers with highly nonlinear cavity dynamics. *Opt. Express* **19**, 8394–8405 (2011).
55. Chen, H.-W. et al. Optimization of femtosecond Yb-doped fiber amplifiers for high-quality pulse compression. *Opt. Express* **20**, 28672–28682 (2012).
56. Dong, L. Nonlinear propagation in optical fibers with gain saturation and gain dispersion. *J. Lightwave Technol.* **38**, 6897–6904 (2020).
57. Rigrod, W. W. Saturation effects in high-gain lasers. *J. Appl. Phys.* **36**, 2487–2490 (1965).
58. Kirsch, D., Bednyakova, A., Cadier, B., Robin, T. & Chernysheva, M. Gain-controlled broadband tuneability in self-mode-locked Thulium-doped fibre laser through variable feedback. figshare https://doi.org/10.6084/m9.figshare.17099657 (2022).

Acknowledgements

D.C.K. and M.C. acknowledge the support of the Deutsche Forschungsgemeinschaft (DFG—German Research Foundation, Project No. CH 2600_1-1). A.B. acknowledges the support of the Ministry of Science and Higher Education of the Russian Federation (Project No. FSUS-2021-0015). A.F. acknowledges the support of the Ministry of Science and Higher Education of the Russian Federation (Project No. 075-15-2021-581) and Russian Science Foundation (Project No. 18-12-00457P).

Author contributions

D.C.K. and M.C. conceived the experiment(s), D.C.K. conducted laser development experiments, A.B. and A.F. built the numerical model, A.B. performed numerical simulations. B.C. and T.R. developed highly Tm-doped fibres. D.C.K., P.V., P.H. and P.P. have investigated gain fibre properties. All authors contributed to results discussions and writing the manuscript.

Funding

Open Access funding enabled and organized by Projekt DEAL.

Competing interests

The authors declare no competing interests.

Additional information

Supplementary information The online version contains supplementary material available at https://doi.org/10.1038/s42005-022-00989-x.

Correspondence and requests for materials should be addressed to Dennis C. Kirsch.

Peer review information *Communications Physics* thanks Xiaomin Liu and the other, anonymous, reviewer(s) for their contribution to the peer review of this work. Peer reviewer reports are available.

Reprints and permission information is available at http://www.nature.com/reprints

Publisher's note Springer Nature remains neutral with regard to jurisdictional claims in published maps and institutional affiliations.